J Therm Anal Calorim (2017) 130:713–720
DOI 10.1007/s10973-017-6435-9

Effect of mechanical activation on the hydrogen reduction kinetics of magnetite concentrate

Ricardo Morales-Estrella[1,2] · Juan Ruiz-Ornelas[1] · Noemi Ortiz-Lara[1] · Yousef Mohassab[2] · Hong Yong Sohn[2]

Received: 8 March 2017 / Accepted: 27 April 2017 / Published online: 11 May 2017

Abstract The effect of mechanical activation on the reduction kinetics of magnetite concentrate by hydrogen was studied. The magnetite concentrate was milled for 8 h in a planetary ball mill. After 8 h of milling, the average particle size was reduced from 14 to 4.4 μm, resulting in a lattice microstrain of 0.3. Isothermal reduction experiments were conducted by thermogravimetry to focus on the chemical reaction as the rate-controlling factor by eliminating external mass transfer effects and using a thin layer of particles to remove interstitial diffusion resistance. Thus, about 2 mg of magnetite powder was reduced at different temperatures under a sufficient flow of hydrogen. The magnetite concentrate and reduction products were analyzed by SEM and XRD. It was found that the onset reduction temperature decreased from 587 to 500 K (314–227 °C) due to the mechanical activation. The activation energy for hydrogen reduction of the activated concentrate decreased about 10% compared with the as-received concentrate. In view of the results, a reaction rate expression was established based on the nucleation and growth model with an Avrami parameter $n = 2.5$.

Keywords Hydrogen reduction · Magnetite · Mechanical activation · Reduction kinetics · Nucleation and growth

✉ Ricardo Morales-Estrella
rmorales@umich.mx

[1] Instituto de Investigación en Metalurgia y Materiales, Universidad Michoacana de San Nicolás de Hidalgo, 58030 Morelia, Michoacán, Mexico

[2] Department of Metallurgical Engineering, University of Utah, Salt Lake City, UT 84112, USA

Introduction

The gaseous reduction of iron oxides is a complex heterogeneous reaction in which the intrinsic rate mechanisms depend upon many parameters such as temperature, type of gaseous reactant and particle size. There is, therefore, extensive research focused on different oxides reduced under different conditions which often lead to discrepancies among published works. Pineau et al. [1] studied the reduction of synthetic magnetite by hydrogen in the temperature range of 483 to 1123 K (210–850 °C). They used about 100 mg of particles with 10–20 μm in diameter. The Arrhenius plot revealed three distinct slopes from which they obtained different apparent activation energies. That is, 200, 71 and 44 kJ mol^{-1} at $T < 523$ K (250 °C), 523 K (250 °C) $< T <$ 663 K (390 °C) and $T > 663$ K (390 °C), respectively. Recently, Elzohiery et al. [2] investigated the reduction kinetics of fine magnetite concentrates using a novel process for rapid reduction; they developed a rate expression for the reduction process and obtained an activation energy value of 193 kJ mol^{-1} in the temperature range of 1423–1623 K (1150–1350 °C).

Mechanical activation is limited to the increase in chemical reactivity of the system, but without altering its chemical composition. The chemical reactivity of powders is increased by inducing physicochemical changes such as size reduction, lattice deformations and decrease in bonding energy by the absorption of mechanical energy. For example, Pourghahramani and Forssberg [3] investigated the effect of mechanical activation on the hydrogen reduction of high-purity hematite. They reported a decrease of 90 K in the onset of the reducing temperature compared with a non-activated sample. In addition, wüstite phase was not detected as an intermediate phase during non-isothermal experiments with heating rates of 10–15 K min^{-1}.

Wüstite is an unstable phase below 843 K (570 °C) under thermodynamic equilibrium.

Several publications have reported that mechanical activation accelerates leaching kinetics [4, 5] of several sulfide and oxide minerals, intensifies oxidation of sulfides [6], and decomposition of sphalerite [7] and chalcopyrite [8]. It has also been demonstrated that mechanical activation allows solid-state reduction of hematite–graphite mixture in an inert atmosphere [9] and the solid-state synthesis of lithium ferrites [10].

As the activation energy is a kinetic measurement, which involves lowest energy pathway in the breaking and forming of chemical bonds, it is thought that the mechanical activation of magnetite concentrate should decrease the energy of metal–oxygen bonds leading to a decrease in the temperature thresholds or energetic of the reactions. Therefore, the objective of this work was to study the effect of mechanical activation on the chemically controlled reduction kinetics of magnetite concentrate by hydrogen.

Experimental

A magnetite concentrate used in this work was obtained from the Mesabi Range, USA. The concentrate is composed of 0.688, 0.041 and 0.271 mass fraction of iron, gangue and removable oxygen, respectively. Argon, helium and hydrogen gases with 99.999% purity were used in the thermogravimetric analysis (TG).

The mechanical activation of magnetite concentrate was induced by dry milling using a planetary ball mill (Retsch PM400) at 300 rpm with grinding times of 1, 2, 4 and 8 h. Stainless steel balls of 10 mm diameter were used as the grinding media; the ball-to-powder ratio was kept at 10:1.

Particle size distribution of the as-received and the milled concentrates was calculated by dynamic light scattering (DLS) using a Coulter LS 100Q. The morphology and chemical analyses of samples were characterized using a scanning electron microscope (SEM) Jeol 6400 in secondary electron image mode equipped with energy-dispersive X-ray spectroscopy (EDS). X-Ray diffraction analysis (XRD) was performed using a Bruker D8 Advance powder diffractometer with Bragg–Brentano geometry. Diffraction patterns were obtained using 40 mA and 40 kV, with a step size of 0.02 degrees and 5 s per step using Cu–Kα radiation and a Ni filter for Fe-fluorescence suppression. Lattice microstrain of the milled samples was computed by Rietveld refinement based on an isotropic microstrain model using TOPAS 4.2 software with fundamental parameters analysis (FPA) provided by Bruker [11].

Thermogravimetric experiments were carried out using a vertical thermogravimetric unit (Setaram, Setsys Evolution 16/18) with a detection limit of 0.03 μg and controlled by a PC interface. Preliminary non-isothermal reduction experiments were conducted at a heating rate of 15 K min^{-1} under a 50% H_2/He atmosphere in order to determine the onset reduction temperature as a function of milling time. Then, isothermal reductions were conducted for both the as-received and the 8-h-milled samples in the temperature range of 673–1173 K (400–900 °C). In order to avoid agglomeration of particles, concentrate particles were dispersed into an alumina crucible with a drop of alcohol and dried at 373 K (100 °C). The crucible containing the sample was of 8 mm inner diameter and 1 mm inner wall height. The temperature inside the reaction chamber was controlled by an S-type Pt–Pt/13% Rh thermocouple located approximately 2 mm below the alumina crucible. Before starting the isothermal reduction experiments, the reaction chamber was evacuated to less 10 Pa and then filled with helium gas up to atmospheric pressure. Isothermal reduction experiments began by heating the reaction chamber to a predetermined reduction temperature at a heating rate of 20 K min^{-1} with a constant helium flow rate of 15 mL min^{-1}. When reduction temperature was stabilized, helium flow was stopped and hydrogen gas was introduced at a constant flow of 120 mL min^{-1} until the sample mass loss remained unchanged. All the thermogravimetric experiments were corrected against the noise generated by the hydrogen flow by running blank experiments under identical conditions. Preliminary isothermal reduction experiments were conducted to establish the optimal experimental parameters to ensure the chemical reaction as the controlling step of the process.

Results and discussion

Magnetite concentrate was subjected to different milling times to decrease particle size and introduce microstrain. Thus, Fig. 1 shows the comparison of the particle size

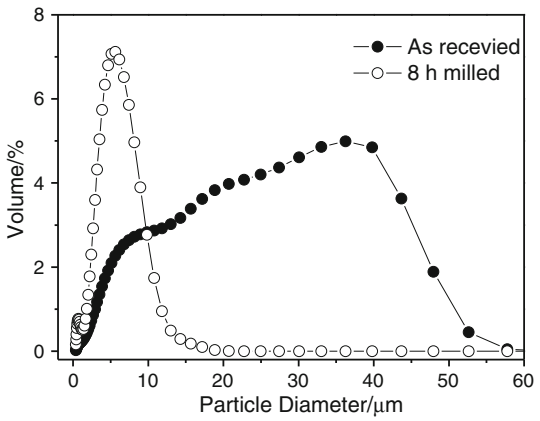

Fig. 1 Particle size distribution of samples studied in this work

distribution of as-received concentrate and the same milled for 8 h. As observed, the as-received powder has a wider particle size distribution with an average size of 14 μm, while the milled powder presents a narrow particle size distribution with an average size of 4.4 μm. Although a uniform particle size is preferable for kinetics analysis, the rate equations can still be applied to particulate ensembles with a distribution of sizes up to a considerable degree of spread [12].

Figure 2 shows the particle morphology change due to milling. The as-received concentrate has angularly shaped particles with noticeable variation in size, while the 8-h-milled concentrate consists of equi-dimensional particles with more homogeneous size distribution which in turn tend to form agglomerates which is common in long dry milling [3]. It can be expected that after the initial fracture into smallest particles, the repeated mechanical deformations caused by high energetic ball–powder–ball and ball–powder–chamber collisions would introduce microstrain into the lattice.

The most direct result of mechanical activation of a dispersed system is determined by an array of physical and physicochemical changes. Table 1 summarizes the changes in physicochemical characteristics by milling. The microstrain contribution in the broadening of the XRD peaks of milled samples was calculated using TOPAS 4.2 software with fundamental parameters analysis (FPA). According to Table 1, it is evident that microstrain increases sharply up to 4 h of milling time; thereafter, the microstrain increases more slowly. From the above results, the sample milled for 8 h was used to study the effect of mechanical activation on the reduction kinetics. For comparison, the as-received concentrate was also studied under similar reducing conditions.

The onset temperature was determined by following the evolution of the first and second derivatives of non-isothermal reduction experiments, under 50% H_2/He, as a function of time. It is clearly seen that mechanical activation does decrease the onset temperature of reduction. Similar results have been reported when mechanically activated hematite was reduced with hydrogen [3]. Furthermore, it has been reported that ball milling of magnesium hydride reduces the hydrogen desorption temperature by 64 K [13]. The fact that mechanical activation decreases the onset temperatures of iron oxide reduction can be attributed to the energy stored in the solid in the form of crystalline defects and strain, and the decrease in the bonding energy of atoms in particles [14]. By the same token, Alex [15] demonstrated that mechanical activation of boehmite led to structural disorder in terms of increased microstrain indicating storage of energy in the solid structure.

Table 1 Physicochemical characteristics of magnetite concentrate with milling time

Milling time/h	Mean size/μm	Median size/μm	Microstrain	Onset temperature/K
As-received	14	16.9	0.0531	587
1	5.6	6.2	0.102	554
2	3.9	4.1	0.199	532
4	3.9	4.1	0.274	519
8	4.4	5	0.307	500

According to the Fe–H–O phase diagram available in the literature [16], the following reactions are expected to occur.

$$\text{At } T < 843\,\text{K}\ (570\,^{\circ}\text{C})$$
$$\text{Fe}_3\text{O}_4 + 4\text{H}_2 \rightarrow 3\text{Fe} + 4\text{H}_2\text{O} \qquad (1)$$
$$\Delta\text{H} = 113.5\,\text{kJ}; K_{\text{eq}} = 3.74\,\text{E} - 5 \text{ at } 673\,\text{K}$$

$$\text{At } T > 843\,\text{K}\ (570\,^{\circ}\text{C})$$
$$(1-x)\text{Fe}_3\text{O}_4 + (1-4x)\text{H}_2 \rightarrow 3\,\text{Fe}_{1-x}\text{O} + (1-4x)\text{H}_2\text{O}\Delta\text{H} = 63.72\,\text{kJ}; K_{\text{eq}} = 0.16 \text{ at } 873\,\text{K} \qquad (2)$$

$$\text{Fe}_{1-x}\text{O} + \text{H}_2 \rightarrow (1-x)\text{Fe} + \text{H}_2\text{O} \qquad (3)$$
$$\Delta H = 16.61\,\text{kJ}; \text{K}_{\text{eq}} = 0.29 \text{ at } 873\,\text{K}$$

To obtain the rate of the chemical reaction as the slowest step in the reduction process, the 8-h-milled sample was tested under isothermal experiments. For example, to

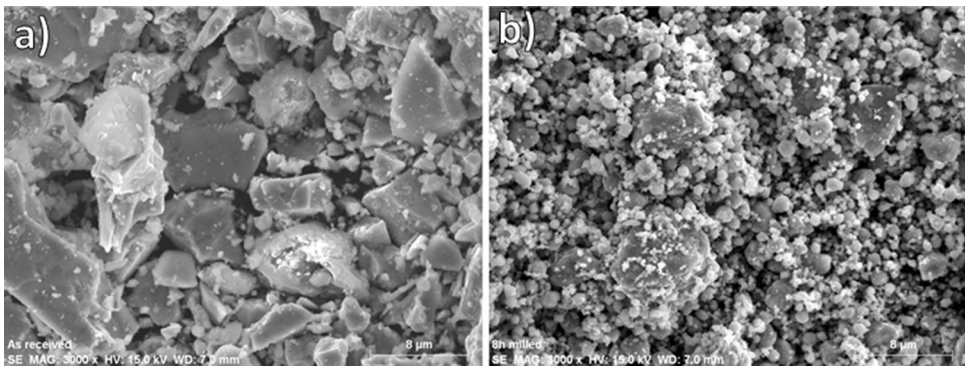

Fig. 2 SEM images showing magnetite concentrate particles: **a** as-received and **b** milled for 8 h

observe the effect of diffusion through the interstices of particles, the mass of the sample was varied as shown in Fig. 3. The fractional reduction, X, was defined as the ratio of the mass loss up to a certain time, Δm_t, over the theoretical final mass loss, Δm_∞, corresponding to the loss of the removable oxygen in the concentrate. From Fig. 4, it can be seen that from about 4 mg and below the reaction rate remains essentially constant. It should be remarked that 2 mg of powder did not cover the whole surface area of the crucible; therefore, 2 mg of powder was considered a small enough amount to avoid interstitial diffusion resistance.

Similarly, to eliminate the effect of external mass transport in the gas phase, different flow rates of hydrogen were tested as shown in Fig. 4. As can be seen, a hydrogen flow rate of 120 mL min^{-1} was sufficient for this purpose.

On the other hand, since the mean particle size for the 8-h-milled concentrate is about 4 μm and a very thin layer of loose particles was used, it is expected that the heat transfer would not be the controlling step even though the endothermic heats of reactions (1) through (3) are appreciable. From the above results, when using about 2 mg of powder and a hydrogen flow rate of 120 mL min^{-1}, the rate-controlling step for reactions (1) through (3) will be the chemical reaction. As aforementioned, all the experiments were corrected against buoyancy effects. Good reproducibility of TG experiments was achieved regardless of the experimental conditions as shown in Fig. 5.

The isothermal reduction curves, X against t, of the 8-h-milled concentrate are shown in Fig. 6. As expected for a chemical-reaction-controlled mechanism, the reduction rate clearly increases with increasing temperature in the lower temperature range, namely, from 673 K (400 °C) to 773 K (500 °C). However, the reduction rate increases

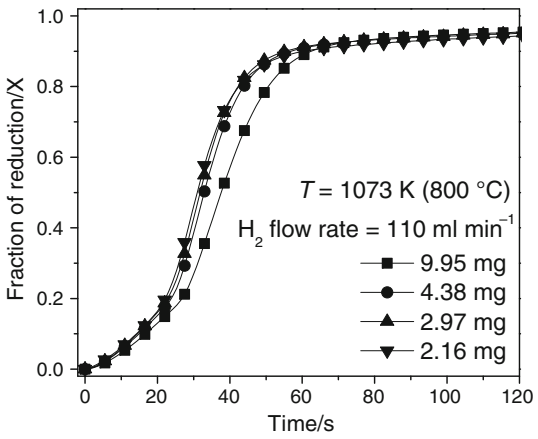

Fig. 3 Effect of the powder layer thickness on the 8-h-milled concentrate reduction

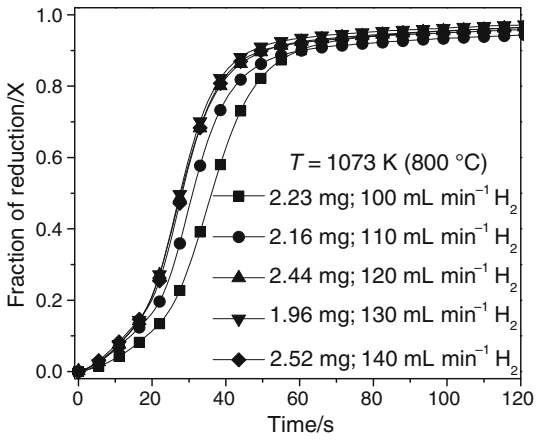

Fig. 4 Effect of hydrogen flow rate on the 8-h-milled concentrate reduction

only slightly from 823 K (550 °C) to 873 K (600 °C); this distinct behavior has been reported in the literature [1, 16, 17] and is attributed to the formation of wüstite [1, 16] as an intermediate reduction phase along with recrystallization and sintering of the metallic iron [17]. Upon further increase in temperature to 973 K (700 °C), the reduction rate becomes slower than at 873 K (600 °C) and the reaction levels off before reaching full conversion. These changes are attributed to significant sintering of particles.

The isothermal reduction experiments with the as-received concentrate are shown in Fig. 7. The reduction curves present the same pattern as the 8-h-milled concentrates shown in Fig. 6 except for the slower reduction kinetics.

All reduction curves present a discontinuity at about $X = 0.10$, which is more noticeable at lower temperatures due to the slower reaction rate. It was found that discontinuity corresponds to the reduction of traces of hematite in the concentrate. The quantitative XRD analysis revealed about 5 mass% of that phase. The exothermic nature of hematite reduction by hydrogen, in contrast to reactions (1) through (3), accounts for the distinct change in the reduction kinetics at early stages.

It is extremely difficult to measure the intrinsic kinetics involving the formation of $Fe_{0.947}O$ and Fe, above 843 K (570 °C) where $Fe_{0.947}O$ is stable, for small particles going through a rapid reduction. In addition, different parts of a small irregular iron oxide particle react at different rates, and thus, different oxide phases may coexist in the particle at any time, which was verified by the XRD analysis of quenched samples by Elzohiery et al. [2]. Therefore, the reduction reaction in this work was treated from a global point of view as the removal of oxygen from iron oxide without distinguishing the stepwise nature even when wüstite is a stable phase. Considering the sigmoidal shape

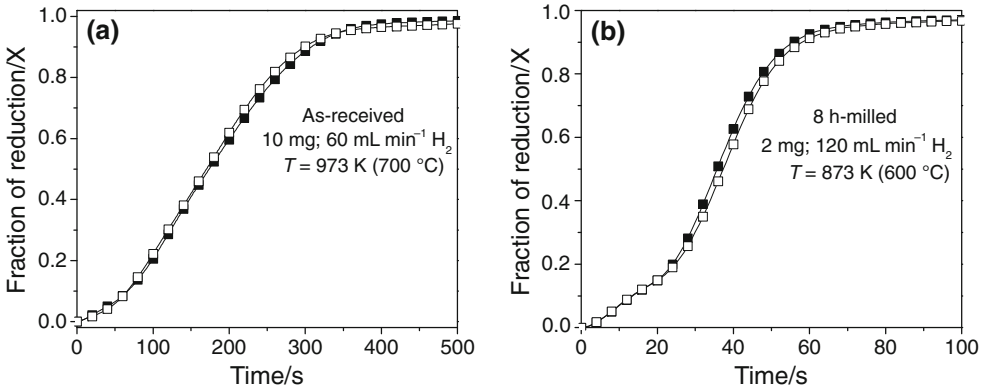

Fig. 5 Reproducibility of TG experiments

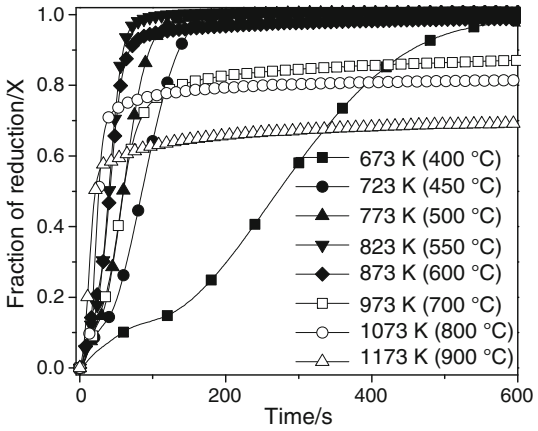

Fig. 6 Effect of temperature on the reduction of 8-h-milled concentrate

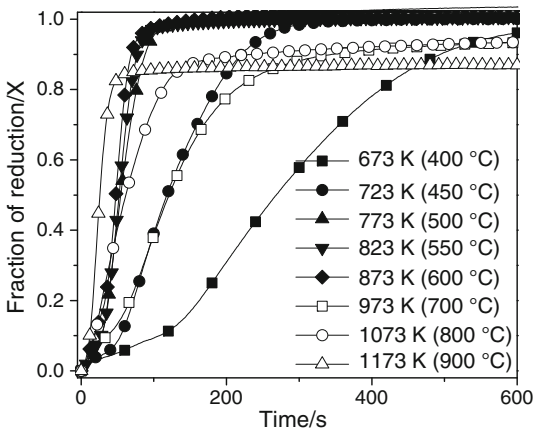

Fig. 7 Effect of temperature on the reduction of the as-received concentrate

of the conversion curve together with the SEM micrographs of particles during the reduction process presented by these authors, the following nucleation and growth rate equation was used to describe the rates of reduction in this work:

$$[-\mathrm{Ln}(1-X)]^{1/n} = k_{\mathrm{app}}t \tag{4}$$

where X is the fractional degree of reduction, t is the reaction time, n is a constant (known as the Avrami parameter [18–20]), and k_{app} is the apparent rate constant which contains the dependence of the rate on gaseous reactant concentration and thus can be written as [2]:

$$k_{\mathrm{app}} = kf(p_{\mathrm{H_2}}, p_{\mathrm{H_2O}}) \tag{5}$$

where k is the intrinsic rate constant, $p_{\mathrm{H_2}}$ and $p_{\mathrm{H_2O}}$ are the hydrogen and water vapor partial pressures in the bulk gas in atm, and f designates the rate dependence on partial pressures. All experiments were conducted in very large excess hydrogen (in this work $p_{\mathrm{H_2O}} \sim 0$), and therefore, the reverse reaction was not considered. Assuming a first-order reaction with respect to hydrogen concentration, namely $f(p_{\mathrm{H_2}}, p_{\mathrm{H_2O}}) = [p_{\mathrm{H_2}} - (p_{\mathrm{H_2O}}/K)]$ being K the equilibrium constant, Eq. (5) yields $k = k_{\mathrm{app}}/[p_{\mathrm{H_2}} - (p_{\mathrm{H_2O}}/K)]$. Furthermore, if the reaction (1) is governed by nucleation and growth phenomena, plotting $\mathrm{Ln}[-\mathrm{Ln}(1-X)]$ against $\mathrm{Ln}(t)$ should yield a straight line with slope n and intercept $n\ \mathrm{Ln}(k_{\mathrm{app}})$. To avoid uncertainties in the calculation of every slope, the earlier stages of reduction were not considered due to the reduction of traces of hematite as discussed above. Also, the decaying periods at later stages of reduction were not taken into account. Therefore, the average value of the Avrami parameter for the 8-h-milled concentrate was $n = 2.5$ as calculated from the slopes in Fig. 8. In this case of the as-received concentrate, the average Avrami parameter obtained from the slopes in Fig. 9 was $n = 2.4$.

SEM analyses were performed to examine the shape of the reduced product and help interpret the observed values of n. As shown in Fig. 10, the product consists mainly of agglomerated spherical particles, but linearly growing iron whiskers were also found. This evidence may explain the average values of the Avrami parameter obtained in the present work, namely, 2.5 and 2.4 for the stressed and the as-received sample, respectively. Considering the above

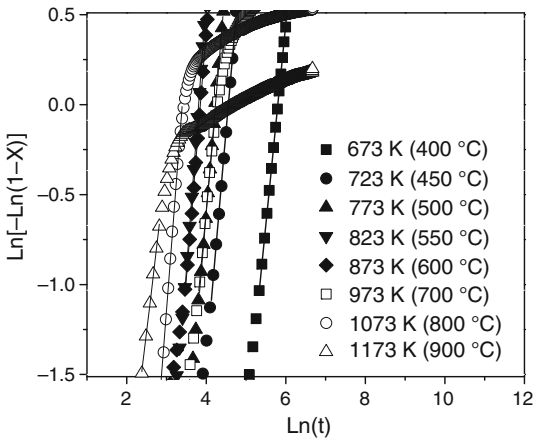

Fig. 8 Determination of the Avrami parameter for the experimental data of the 8-h-milled concentrate

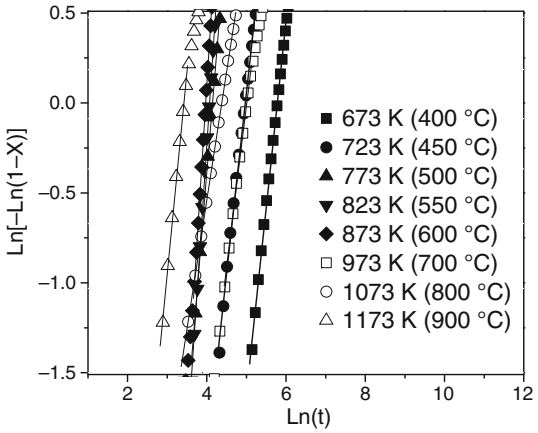

Fig. 9 Determination of the Avrami parameter for the experimental data of the as-received concentrate

results, an Avrami parameter of 2.5 was used in Eq. (4) for the reduction kinetics analysis.

Thus, the values of apparent rate constant, k_{app}, for the 8-h-milled and the as-received concentrates were obtained from the slopes of Figs. 11 and 12, respectively. As mentioned above, the initial and later stages of reduction were neglected. Using Eq. (5), the intrinsic rates constants were calculated and plotted against the inverse of temperatures, as shown in Fig. 13.

From the Arrhenius plot, it can be realized that the intrinsic rates seem to fit different slopes. Similar results have also been reported in Ref. [1]. The rate constants, corresponding to higher temperatures, were left out from the calculation of the activation energy as they are greatly affected by sintering. The computed values of the activation energy, in the temperature range of 673 to 823 K (400–550 °C), were 70 and 65 kJ mol^{-1} for the as-received concentrate and the mechanically activated concentrate, respectively. Other authors have also documented a decrease in the activation energy of samples subjected to mechanical milling [3, 13, 21, 22]. The activation energies thus obtained correspond to the chemical reaction as the rate-controlling mechanism since those intrinsic rate constants were sensitive to temperature increase, while sintering of the particles is likely to be negligible for the considered temperature range. Further, the above temperature range also lies below the formation of wüstite as an intermediate phase. An activation energy value of 88 kJ mol^{-1} has been reported for the reduction of iron oxide in the literature with nucleation and growth as the controlling mechanism [23]. The difference in the activation energies should be attributed to the mechanical activation alone and not to the difference in particle size. A change in particle size can change the intrinsic rate but not the value of activation energy.

The rate of reaction for both magnetite concentrates is given by

$$dX/dt = (5/2)k[-\mathrm{Ln}(1-X)]^{3/5}(1-X)\,[p_{H_2} - (p_{H_2O}/K)] \tag{6}$$

where

$$k = 371\ \exp\left(-65\ \text{kJ mol}^{-1}/RT\right) \quad \text{for the 8 h milled concentrate and} \tag{7}$$

$$k = 663\ \exp\left(-70\ \text{kJ mol}^{-1}/RT\right) \quad \text{for the as-received concentrate.} \tag{8}$$

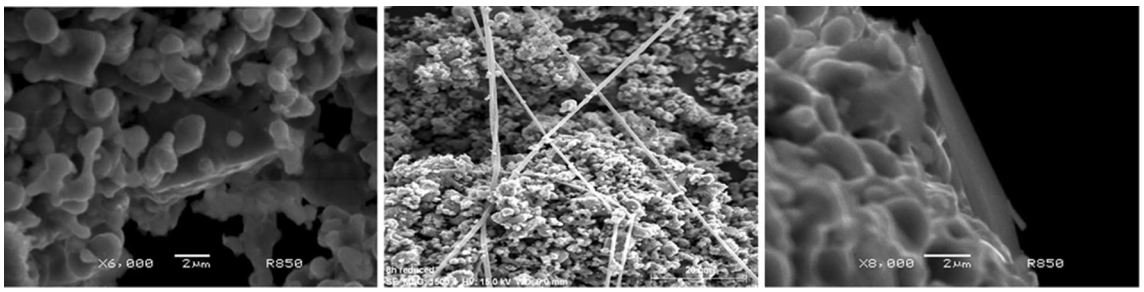

Fig. 10 SEM images of 8-h-milled concentrate reduced at 1123 K (800 °C)

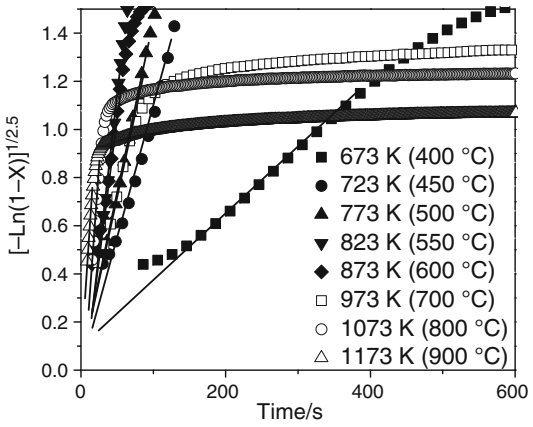

Fig. 11 Determination of the apparent rate constant for 8-h-milled concentrate using $n = 2.5$

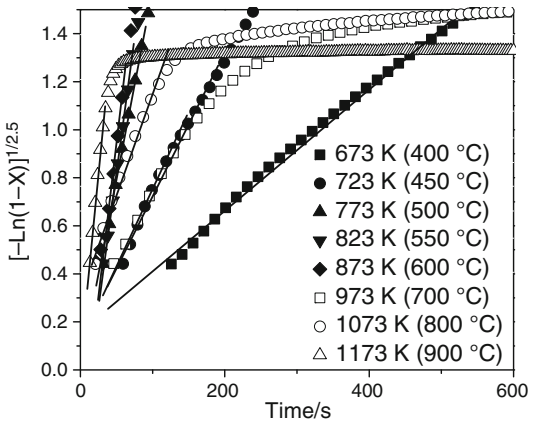

Fig. 12 Determination of the apparent rate constant for the as-received concentrate using $n = 2.5$

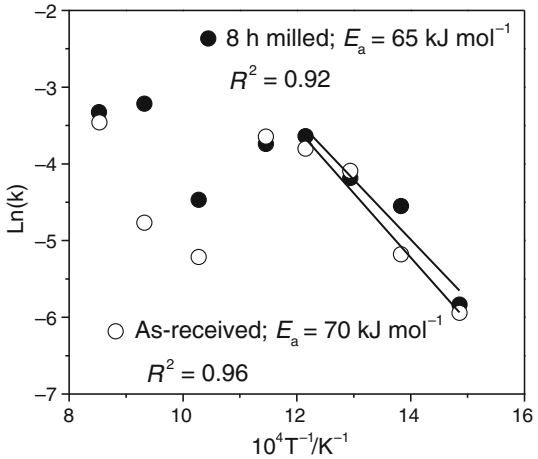

Fig. 13 Arrhenius plot for the as-received concentrate and the 8-h-milled concentrate

Conclusions

In the present work, the mechanically activated concentrate with a lattice microstrain of 0.30 led to a lower onset temperature of reduction compared with the as-received sample, namely, from 587 to 500 K (314–227 °C). Under the experimental conditions, noticeable sintering of particles was observed in the thermogravimetric experiments at and above 973 K (700 °C). The SEM analyses on the reduction products from the activated concentrate revealed the presence of spherical particles and traces of whiskers. The activation energies were calculated based on the nucleation and growth model when the rate of chemical reaction is the controlling mechanism, in the temperature range 673–773 K (400–500 °C), leading to 70 kJ mol^{-1} and 65 kJ mol^{-1} for the as-received concentrate and the mechanically activated concentrate, respectively. The rate of conversion for the hydrogen reduction of magnetite concentrate by hydrogen was developed with an Avrami parameter of $n = 2.5$. The mechanical milling decreases the particle size and generates lattice strain in the bulk of the particles; as a result, less energy is required for the breakage of the metal–oxygen bonds by hydrogen and consequent transformation to metallic iron. Therefore, the reduction reaction is achieved at a lower temperature compared with the non-activated concentrate.

Acknowledgements Support from the National Council for Science and Technology, CONACYT Mexico, for one of the authors (J. Ruiz) is gratefully acknowledged.

References

1. Pineau A, Kanari N, Gaballah I. Kinetics of reduction of iron oxides by H2. Part II. Low temperature reduction of magnetite. Thermochim Acta. 2007;456:75–88.
2. Elzohiery M, Sohn HY, Mohassab Y. Kinetics of hydrogen reduction of magnetite concentrate particles in solid state relevant to flash ironmaking. Steel Res Int. 2016;1600133:1–14.
3. Pourghahramani P, Forssberg E. Effects of mechanical activation on the reduction behavior of hematite concentrate. Int J Miner Process. 2007;82:96–105.
4. Baláž P. Influence of solid state properties on ferric chloride leaching of mechanically activated galena. Hydrometallurgy. 1996;40:359–68.
5. Tkacova K, Balaz P, Misura B, Vigdergauz VE, Chanturiya VA. Selective leaching of zinc from mechanically activated complex CuPbZn concentrate. Hydrometallurgy. 1993;33:291–300.
6. Chen Q, Hu H, Yin Z, Zhang P, Ye L. The oxidation behavior of unactivated and mechanically activated sphalerite. Metall Mater Trans B. 2002;33:897–900.
7. Balaz P, Ebert I. Thermal decomposition of mechanically activated sphalerite. Thermochim Acta. 1990;180:117–23.
8. Tkacova K, Balaz P, Bastl Z. Thermal characterization of changes in structure and properties of chalcopyrite after mechanical activation. Thermochim Acta. 1990;170:277–88.

9. Tahmasebi R, Shamanian M, Abbasi MH, Panjepour M. Effect of iron on mechanical activation and structural evolution of hematite–graphite mixture. J. Alloys Compd. 2009; 472:334–42.
10. Lysenko EN, Surzhikov AP, Vlasov VA, Malyshev AV, Nikolaev EV. Thermal analysis study of solid-phase synthesis of zinc- and titanium-substituted lithium ferrites from mechanically activated reagents. J Therm Anal Calorim. 2012;122:1347–53.
11. Bruker AXS. TOPAS V4: General profile and structure analysis software for powder diffraction data. User's Manual. Karlsruhe, Germany: Bruker AXS GmbH; 2009.
12. Cho J, Sohn HY. Effects of particle shape and size distribution on the overall fluid-solid reaction rates of particle assemblages. Can J Chem Eng. 2016;94:1516–23.
13. Huot J, Liang G, Boily S, Van Neste A, Schulz R. Structural study and hydrogen sorption kinetics of ball-milled magnesium hydride. J. Alloys Compd. 1999;293:495–500.
14. Juhász Z, Opoczky L. Mechanical activation of minerals by grinding: pulverizing and morphology of particles. Akadémiai Kiadó; 1990.
15. Alex TC. An insight into the changes in the thermal analysis curves of boehmite with mechanical activation. J Therm Anal Calorim. 2014;117:163–71.
16. Pineau A, Kanari N, Gaballah I. Kinetics of reduction of iron oxides by H2. Part I: Low temperature reduction of hematite. Thermochim Acta. 2006;447:89–100.
17. Edstrom JO. The mechanism of reduction of iron oxides. J. Iron Steel Inst. 1953;175:289–304.
18. Avrami M. Kinetics of phase change. I general theory. J Chem Phys. 1939;7:1103–12.
19. Avrami M. Kinetics of phase change. II transformation-time relations for random distribution of nuclei. J Chem Phys. 1940;8:212–24.
20. Avrami M. Granulation, phase change, and microstructure kinetics of phase change. III. J Chem Phys. 1941;9:177–84.
21. Varin RA, Bidabadi AS. The effect of milling energy input during mechano-chemical activation synthesis (MCAS) of the nanocrystalline manganese borohydride ($Mn(BH_4)_2$) on its thermal dehydrogenation properties. Int J Hydrog Energy. 2014;39:11620–32.
22. Udhayabanu V, Singh N, Murty BS. Mechanical activation of aluminothermic reduction of NiO by high energy ball milling. J Alloys Compd. 2010;497:142–6.
23. Junca E, Guisard Restivo TA, de Oliveira JR, Romano Espinosa DC, Soares Tenório JA. Reduction of electric arc furnace dust pellets by simulated reformed natural gas. J Therm Anal Calorim. 2016;126:1889–97.